A potential wasteform for Cs immobilization: synthesis, structure determination, and aqueous durability of Cs2TiNb6O18

CHEN, Tzu-Yu, MADDRELL, Ewan R., HYATT, Neil C. and HRILJAC, Joseph A.

Published version

CHEN, Tzu-Yu, MADDRELL, Ewan R., HYATT, Neil C. and HRILJAC, Joseph A. (2016). A potential wasteform for Cs immobilization: synthesis, structure determination, and aqueous durability of Cs2TiNb6O18. Inorganic Chemistry, 55 (24), 12686-12695.

Inorganic Chemistry

Article

pubs.acs.org/IC

A Potential Wasteform for Cs Immobilization: Synthesis, Structure Determination, and Aqueous Durability of $Cs_2TiNb_6O_{18}$

Tzu-Yu Chen,*[,†] Ewan R. Maddrell,[‡] Neil C. Hyatt,[§] and Joseph A. Hriljac*[,†]

[†]School of Chemistry, University of Birmingham, Edgbaston, Birmingham B15 2TT, United Kingdom

[‡]National Nuclear Laboratory, Workington, Cumbria CA14 3YQ, United Kingdom

[§]Department of Materials Science and Engineering, University of Sheffield, Sir Robert Hadfield Building, Mappin Street, Sheffield S1 3JD, United Kingdom

Supporting Information

ABSTRACT: $Cs_2TiNb_6O_{18}$ is a potential ceramic wasteform for the long-term immobilization of radioactive cesium. $Cs_2TiNb_6O_{18}$ was synthesized using the aqueous precursor method and a solid-state reaction, and its crystal structure was determined from the Rietveld refinement of synchrotron X-ray and neutron powder diffraction data. The structure is a pyrochlore analogue, space group $P\bar{3}m1$ with Cs in 9-fold coordination. The calculated bond valence sum from analysis of neutron diffraction data of 0.84 and high coordination number suggest that Cs has a strong bonding environment. The chemical aqueous durability was investigated using the MCC-1 and PCT-B standard test methods. The measured Cs leach rates of 3.8×10^{-3} and 2.1×10^{-3} g m^{-2} day^{-1} obtained via the MCC-1 and PCT-B methods, respectively, demonstrate good promise of a safe long-term immobilization material comparable to, if not better than, hollandite—the material in the multiphase titanate ceramics (Synroc) targeted for cesium sequestration.

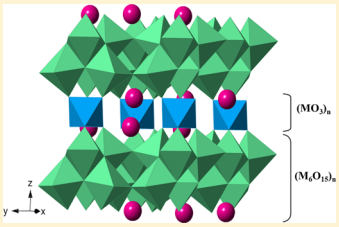

INTRODUCTION

Several radioisotopes of cesium are produced during uranium fission, and three remain after spent fuel discharge: ^{134}Cs, ^{135}Cs, and ^{137}Cs with half-lives of 2.1, 2.3 million, and 30.2 years, respectively. ^{137}Cs and ^{90}Sr, medium-life fission products, account for the majority of radiation from spent fuel between a few and a few hundred years after use. ^{137}Cs is the main medium-term health risk remaining from the Chernobyl and Fukushima accidents, as cesium can biologically substitute for potassium in living organisms. In addition, most common cesium compounds are water-soluble and will transport rapidly in the environment with groundwater. It has been estimated that the Fukushima accident released approximately 10 PBq of ^{137}Cs into the environment with approximately 10% of that deposited on land in Japan.[1−3] The removal of this radionuclide from the environment continues to be a large part of the cleanup effort, with the main route being removal by inorganic ion exchange materials. After use, these low-density materials are classified as high-level waste and are currently being stored on site. Clearly a better situation would be the safe conversion to either a glass or ceramic wasteform with a higher density and lower potential for release of the cesium back into the environment due to degradation/leaching.

Ceramic hosts generally possess far superior chemical durabilities in comparison to glass and better flexibility to incorporate complicated chemical species within the lattices; a number of crystalline ceramic materials such as apatite-, pollucite-, and titanate-based compounds have been explored for the immobilization of cesium. Hollandite, one of the major titanate phases in Synroc, has been widely studied and is considered one of the best materials. Hollandite has a general formula of $A_xB_yC_{8-y}O_{16}$ where $x \leq 2$, the A site is occupied by large monovalent and/or divalent cations (e.g., Cs^+ and Ba^{2+}), and the B and C sites contain octahedrally coordinated cations such as Ti^{4+} and Al^{3+} with a valence between 2 and 5. In spite of the relatively open framework type structure of (Ba, Cs) hollandite, the large Ba^{2+} and Cs^+ cations are securely locked within the tunnels surrounded by eight oxygen anions, forming a cage that due to the relatively high bonding energy inhibits their free migration. Many studies throughout the years have also demonstrated that the ability of hollandite to immobilize cations over a wide compositional range is likely due to the low ionic conductivity of the cations in the tunnels.[4−7]

The other advantage of hollandite is that it is a natural electron trap when cesium radioactively decays to barium with reduction of Ti(IV) into Ti(III) or Fe(III) into Fe(II). However, radiation stability is still also of concern. Although hollandite phases do not host actinides, in a multiphase ceramic system it will also experience irradiation from α particles emitted in adjacent actinide-containing phases. When hollandite is irradiated by heavy ions, an expansion in the unit cell volume and a structural transformation from tetragonal to a lower symmetry monoclinic structure, or even an amorphization, can occur.[8,9] The anisotropy of the unit cell expansion causes an increase in the size of the channels along the c axis, which could significantly affect the ability of the barium hollandite structure to retain Cs cations in an aqueous environment.[10]

Received: August 3, 2016
Published: November 29, 2016

DOI: 10.1021/acs.inorgchem.6b01826
Inorg. Chem. 2016, 55, 12686−12695

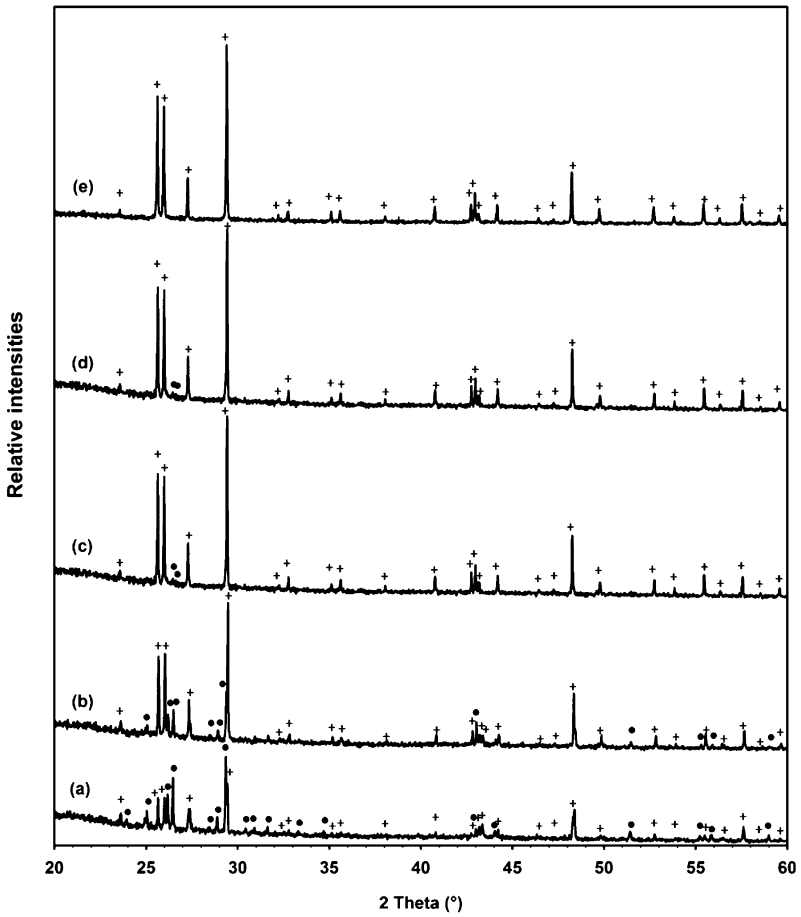

Figure 1. (a–d) XRD patterns showing the phase growth of $Cs_2TiNb_6O_{18}$ after one to four times of sintering using the solid-state route. (e) XRD pattern of $Cs_2TiNb_6O_{18}$ using an aqueous precursor route. The + and ● symbols denote the positions of the peaks according to ICDD PDF 01-070-0674 ($Cs_2TiNb_6O_{18}$) and 00-005-0379 (Nb_2O_5), respectively.

Table 1. XRF Results of $Cs_2TiNb_6O_{18}$ Synthesized via a Solid-State Reaction and the Aqueous Precursor Route

	theoretical		solid state		aqueous precursor	
element	wt %	atom %	wt %	atom %	wt %	atom %
Cs	22.93	7.41	23.14 ± 0.28	7.47	21.29 ± 0.22	6.83
Ti	4.13	3.70	4.37 ± 0.67	3.91	4.13 ± 0.53	3.66
Nb	48.09	22.22	47.68 ± 0.04	22.02	49.31 ± 0.03	22.52

There is a need to develop new geochemically stable materials in the disposal environment to ensure a safer cesium fixation.

IONSIV IE-911 is a material commercially available from UOP and has been used to remove cesium from wastewater in the Fukushima efforts as well as at several Magnox storage ponds in the U.K. and various US locations, including Three Mile Island, Savannah River, and Oak Ridge National Laboratory.[11,12] In previous work[13] we showed that hot isostatic pressing of Cs-exchanged IONSIV IE-911 leads to a dense mixture of ceramic phases with the cesium partitioning into $Cs_2TiNb_6O_{18}$ at lower exchange levels and then a mixture of $Cs_2TiNb_6O_{18}$ and $Cs_2ZrSi_6O_{15}$ at higher exchange levels. $Cs_2TiNb_6O_{18}$ is a pyrochlore analogue first reported by Desgardin et al.[14] in 1977 but has been little researched since then. These workers also studied related phases of composition $A_2B_6TiO_{18}$ (A = Cs, Rb, Tl, and B = Ta, Nb) with an interest in ionic conductivity.[15] Other materials with the pyrochlore structure have been studied as ceramic wasteforms for radionuclides, as they have a good coordination environment for large

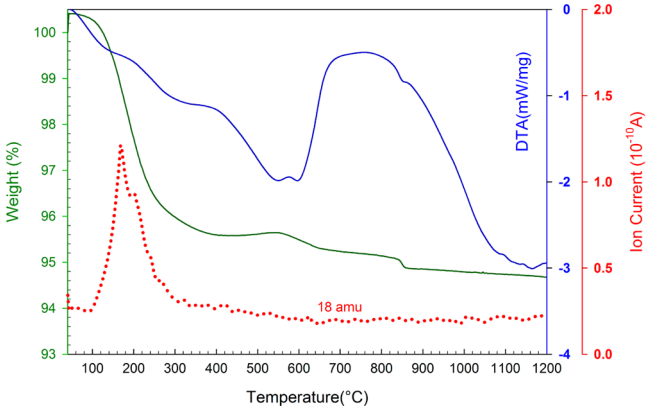

Figure 2. TG/DTA/MS plot for the reaction of the aqueous precursor converting to $Cs_2TiNb_6O_{18}$.

cations such as cesium and actinides.[16−19] The focus of this work is to study in detail the crystal structure and aqueous

DOI: 10.1021/acs.inorgchem.6b01826
Inorg. Chem. 2016, 55, 12686−12695

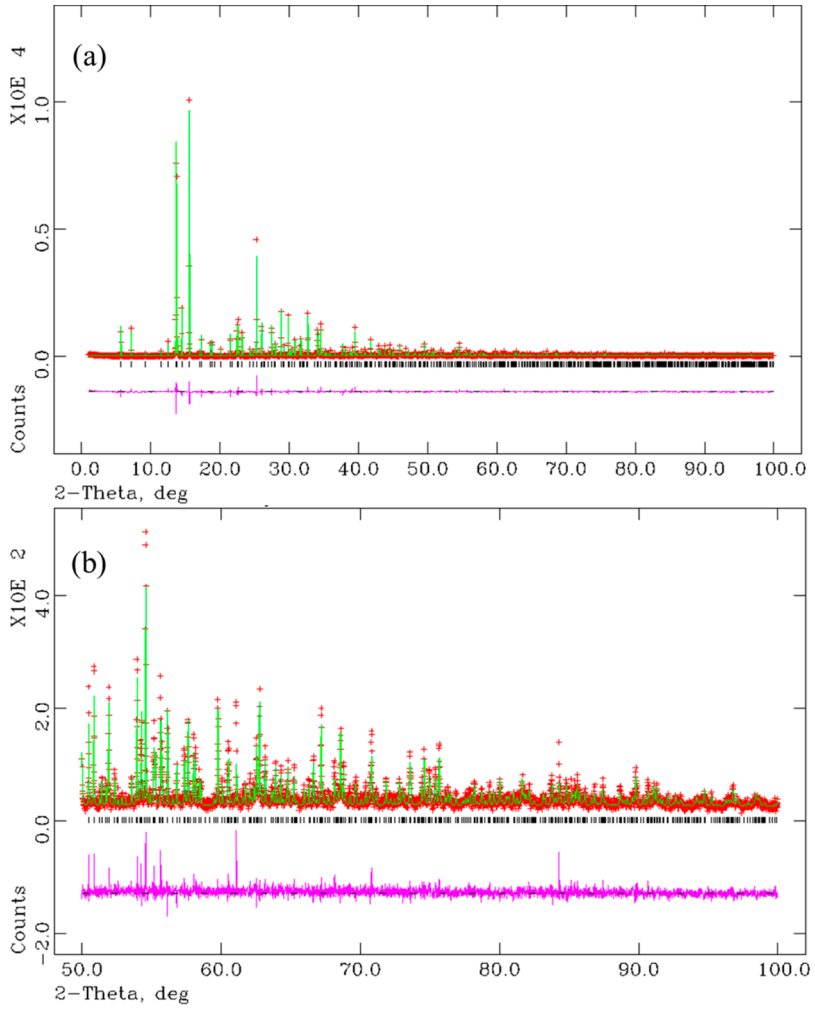

Figure 3. Simulated (green line) and experimental diffraction patterns (red dots) as well as difference pattern (purple) for $Cs_2TiNb_6O_{18}$ (aqueous route) using synchrotron X-ray diffraction data: (a) 2θ 0−100°; (b) 2θ 50−100°.

Table 2. Refinement Parameters, Unit Cell Parameters, Refined Atom Positions, Occupancies, and Isotropic Displacement Parameters from the Refinement of Synchrotron PXRD for $Cs_2TiNb_6O_{18}$ Synthesized via the Aqueous Precursor Method

Refinement and Lattice Parameters			
refinement param		lattice param	
R_{wp}/%	17.53	a/Å	7.53923(2)
R_p/%	12.96	c/Å	8.19426(3)
χ^2	3.027	V/Å^3	403.361(2)

Refined Atom Positions, Multiplicities, Occupancies, and Isotropic Displacement Parameters						
	x	y	z	mult	occ[a]	U_{iso}(Å^2)
Cs1	0.3333	0.6667	0.63393(17)	2	1	0.0198(3)
Nb1	0	0	0.5	1	0.743(8)	0.0076(5)
Ti1	0	0	0.5	1	0.257(8)	0.0076(5)
Nb2	0.16934(6)	−0.16934(6)	0.14599(11)	6	0.876(1)	0.0018(1)
Ti2	0.16934(6)	−0.16934(6)	0.14599(11)	6	0.124(1)	0.0018(1)
O1	0.4481(4)	−0.4481(4)	0.1640(7)	6	1	0.0013(6)
O2	0.8575(4)	−0.8575(4)	0.0972(7)	6	1	0.0013(6)
O3	0.1234(4)	−0.1234(4)	0.3609(8)	6	1	0.0013(6)

[a]Site occupancies for sites Nb1/Ti1 and Nb2/Ti2 both constrained to sum to 1.

leaching behavior of $Cs_2TiNb_6O_{18}$ to assess its suitability as a ceramic wasteform.

$Cs_2TiNb_6O_{18}$ can be synthesized via a solid-state reaction, the easiest and most straightforward way as reported by Desgardin et al.[14] However, due to the potential volatility of cesium compounds at high temperature, a solid-state reaction which requires high firing temperature and long duration is not ideal. Alternatively, an aqueous precursor route, which creates

DOI: 10.1021/acs.inorgchem.6b01826
Inorg. Chem. 2016, 55, 12686−12695

Table 3. Interatomic Cs−O, Ti−O, and Nb−O Distances (Å) in $Cs_2TiNb_6O_{18}$ (Aqueous Precursor Route) Calculated on the Basis of the Refinement Result using Synchrotron X-ray Diffraction Data

atoms		bond length/Å	mean distance/Å	valence sum (vu)	coordination
Cs1	O1	3.300(5) (×3)	3.39 (for 9 existing Cs−O bonds)	0.76	9
Cs1	O2	3.326(5) (×3)			
Cs1	O3	3.538(5) (×3)			
Cs1	O3	3.8115(7) (×2)[a]	3.56 (for all Cs−O bonds)		
Cs1	O3	3.8123(7) (×2)[a]			
Cs1	O3	3.8120(7) (×2)[a]			
Nb1	O3	1.974(6)(×6)	1.98	5.05	6
Ti1	O3	1.974(6)(×6)	1.98	3.89	6
Nb2	O1	1.909(1) (×2)	1.98	5.10	6
Nb2	O2	2.098(2) (×2)			
Nb2	O2	2.023(6) (×1)			
Nb2	O3	1.861(6) (×1)			
Ti2	O1	1.909(1) (×2)	1.98	3.94	6
Ti2	O2	2.098(2) (×2)			
Ti2	O2	2.023(6) (×1)			
Ti2	O3	1.861(6) (×1)			
				av bond valence sum (vu)	
	Nb			5.08	
	Ti			3.92	

[a]Distances considered too long for bonds.

precipitation of cations as an intimate mixture of alkoxides, may be preferable. Although the method is generally well developed, the use of metal alkoxides for $Cs_2TiNb_6O_{18}$ synthesis has never been explored. In this work, an easy to control and efficient method for producing $Cs_2TiNb_6O_{18}$ using an aqueous precursor is reported and the product compared to one made by a conventional ceramic process. Structures were refined using the Rietveld method with both TOF neutron and synchrotron X-ray powder diffraction data. The chemical durability of monolithic and powdered specimens to Cs release in an aqueous environment was also measured. The viability of $Cs_2TiNb_6O_{18}$ as a potential wasteform for cesium immobilization is thus evaluated.

EXPERIMENTAL SECTION

Sample Preparation. Powder samples of $Cs_2TiNb_6O_{18}$ were successfully prepared via both solid-state and aqueous precursor synthesis methods. For solid-state synthesis, Cs_2CO_3, TiO_2, and Nb_2O_5 with a Cs:Ti:Nb molar ratio of 2:1:6 were ground to mix, pressed into pellets, and then calcined at 1200 °C for 13 h. Repeating grinding and sintering steps were required to increase the amount and purity of the product.

For the aqueous precursor synthesis, the method was modified from the literature procedure reported by Balmer et al.[20] for $Cs_2ZrSi_3O_9$ synthesis. A solution was prepared by mixing a 50 wt % aqueous solution of cesium hydroxide (CsOH) with an equal volume of ethanol. One milliliter aliquots of the CsOH/ethanol solution were injected into a mixture of titanium isopropoxide and niobium ethoxide with stirring, followed by the injection of 1 mL of ethanol. The injections of CsOH/ethanol and ethanol were repeated until the CsOH/ethanol was used up. Then extra 2 mL portions of ethanol and water were added to the mixture. The concentrations of the reactants were based on a final Cs:Ti:Nb cation ratio of 2:1:6. The mixture was aged overnight and then dried in an oven at 100 °C. The precursor was then ground and pressed into pellets; these were placed in a platinum crucible and heated in air at a rate of 10 °C/min to 1200 °C and held for 15 h.

Characterizations. Fused borate glass beads were used for the determination of elemental compositions using X-ray fluorescence spectrometry (Bruker S8 Tiger WDXRF). Circular glass beads with flat surfaces were prepared by heating ground mixtures of sample and lithium tetraborate in a 1:10 ratio to 1050 °C in a platinum crucible. A nonwetting agent, ammonium iodide (NH_4I), was added to help the bead exfoliate from the crucible. Thermogravimetric analysis and differential thermal analysis (TGA/DTA) experiments with mass spectral analysis were performed on a NETZSCH STA 449FA instrument. A sample precursor which had been dried overnight was heated to 1000 °C at a heating rate of 10 °C/min under an oxygen atmosphere. Laboratory powder X-ray diffraction (PXRD) patterns were collected from 5 to 90° in 2θ with a Bruker D8 Advance diffractometer operating in transmission mode using Cu Kα radiation (λ = 1.5406 Å) and a LynxEye detector. An absorption correction was applied to the raw data prior to analysis using the Rietveld method.

Synchrotron (I11, Diamond, U.K.) and neutron (GEM, ISIS, U.K.) powder diffraction data sets of $Cs_2TiNb_6O_{18}$ were collected. Rietveld refinements of the synchrotron and neutron diffraction data were performed using the General Structure Analysis System (GSAS) program.[21] The starting values of the atomic positions, lattice parameters, and displacement parameters for the $Cs_2TiNb_6O_{18}$ framework were taken from the literature.[14] The atomic positions and isotropic displacement parameters (U_{iso}) of Ti and Nb which share the same site were constrained. The U_{iso} values for all of the oxygen atoms were considered to be the same. The occupancies of the Cs and Ti/Nb sites were also refined. Bond valence sums were determined by the method of Brown and Altermatt.[22]

For synchrotron data, the specimen displacement and lattice parameters were refined after zero and scale factor had converged and the background was graphically fitted. Then, the peak profiles were fitted to symmetric pseudo-Voigt functions (Type 3). GU, GV, and GW were first refined for Gaussian coefficients, and LX and LY were then

DOI: 10.1021/acs.inorgchem.6b01826
Inorg. Chem. 2016, 55, 12686−12695

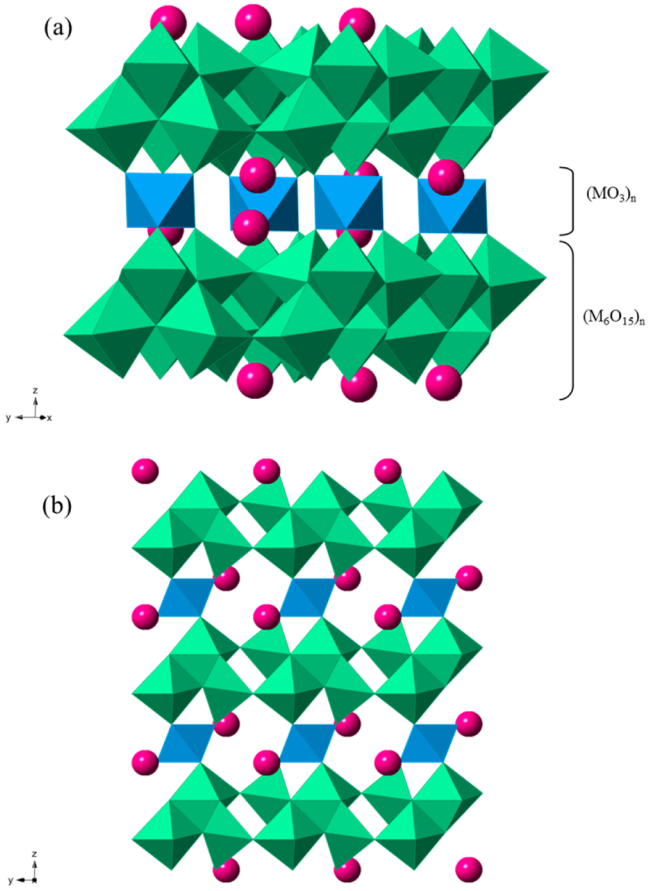

Figure 4. Polyhedral (Ti/Nb) representations of $Cs_2TiNb_6O_{18}$: (a) view through the [100] direction; (b) view along the x axis. Blue octahedra correspond to site 1 and green to site 2, and pink spheres represent Cs atoms.

refined for Lorentzian coefficients. After a satisfactory profile was achieved, the effect of preferred orientation was refined.

Chemical Durability. Static leaching tests were carried out using both the 1998 MCC-1[23] and 2002 PCT-B[24] standard methods. First some of the material made by the aqueous precursor route was packed in a mild steel can and hot isostatically pressed at 190 MPa and 1100 °C for 2 h to produce a dense ceramic. Thin slices were cut, and the resultant monolithic specimens were dry-polished to a standard 600 grit surface finish. For PCT-B tests, the ceramic was ground and sieved to 75−150 μm. The sieved ceramic was washed with ASTM type I water and ethanol to remove adhering fines. Cleaned samples were placed in a 90 ± 10 °C oven overnight to dry before the test. For MCC-1 tests, monolithic specimens of known geometric surface area were immersed in DI water in Teflon pots for periods ranging from 3 to 28 days without agitation at 90 °C. The surface area to leachant volume (SA/V) ratio was held constant within 0.5 of 10 m^{-1}. For PCT-B tests, a 1 g portion of sample and 10 mL of leachant were sealed in the vessel. The estimated ratio of surface area to leachant volume is around 1224 m^{-1}. Tests for each sample were carried out in triplicate, and two vessel blanks from the same batch were used. Samples and blanks were placed in the oven at 90 °C for 7 days. Solutions were passed through a 0.45 μm syringe filter, and element concentrations were detected using ICP-MS (Agilent 7500ce).

The normalized leach rate is given by the relation

$$(\mathrm{NR})_i = \frac{(C_{ij} - B_i) \times V_j}{f_i \times \mathrm{SA} \times t}$$

where C_{ij} is the concentration of element i observed in the leachate from specimen j, averaged over replicate aliquots, B_i is the average concentration of element i observed in the leachate from the blank, averaged over replicate aliquots and blanks, V_j is the initial volume of leachate in test vessel containing specimen j, f_i is the mass fraction of element i in the unleached specimen, SA is the specimen surface area in m^2, and t is the duration of the leach test in days.

RESULTS AND DISCUSSION

Optimisation of Synthesis. $Cs_2TiNb_6O_{18}$ has been successfully synthesized using both ceramic solid-state reactions and the aqueous precursor method. The diffraction patterns shown in Figure 1a−d reveal the phase growth of $Cs_2TiNb_6O_{18}$ with four repeated sinterings of a solid-state reaction, and a highly crystalline end product was obtained. A very small amount of an impurity was found in the final product, likely unreacted Nb_2O_5 (it has a complicated monoclinic unit cell, and so it is difficult to unambiguously confirm due to reflection overlap). An attempt was made to identify it from a back-scattered SEM image (Supporting Information), but it could not be observed. The need for several high-temperature firings introduced the risk of Cs loss due to its volatility; therefore, a second sample was made using an aqueous precursor route. In this case, a highly crystalline and pure product was successfully made in one firing, as shown in Figure 1e. The advantages of the aqueous precursor method for this phase are therefore ease of composition control, reduced firing duration, and high quality of the final product. The compositions of both samples were determined using XRF, as shown in Table 1, and the results are consistent with phase-pure materials. For the ceramic sample, the atomic ratio Cs:(Ti + Nb) is 2.03:7, and for the material made by the aqueous precursor route it is 1.82:7. This is suggestive of a slight Cs deficiency for the latter, although likely this is just at the margins of the accuracy of the determination.

Thermal Analysis. The thermal behavior of the precursor was studied using thermogravimetric analysis with mass spectral monitoring of the evolved gases, as shown in Figure 2. The majority of the weight loss (4.77%) occurred below 600 °C and is attributed mainly to the removal of molecular water (<400 °C). This is supported by the mass spectral monitoring of H_2O emissions at 18 amu. The large exothermic event in the DTA curve starting around 600 °C is attributed to the crystallization of $Cs_2TiNb_6O_{18}$.

Rietveld Structure Refinement. A high-resolution synchrotron X-ray powder diffraction pattern of the sample made via the aqueous precursor route was collected and analyzed using the Rietveld method, and an excellent fit was obtained, as shown in Figure 3; the refinement results are presented in Tables 2 and 3. $Cs_2TiNb_6O_{18}$ crystallizes in the trigonal system $P\bar{3}m1$, and the refined unit cell parameters a and c are 7.53923(2) and 8.19426(3) Å, respectively, consistent with those previously reported.[14] The Nb and Ti atoms are disordered over two crystallographically distinct sites, as shown in Figure 4. Completely random occupancies would correspond to site fractions of 0.857 and 0.143 for Nb and Ti, respectively. The refined values suggest a slight preference for Ti site 1, labeled as $(MO_3)_n$ in Figure 4a. Neutron diffraction data were collected at room temperature on the sample prepared by the ceramic route in order to further probe the Cs content and Ti/Nb ordering and better define the oxygen position. The scattering contrast of Ti vs Nb is much greater for neutrons, −3.438 and 7.054 fm,[25] than for X-rays, 18 (Ti^{4+}) and 38 electrons (Nb^{5+}). The model was simultaneously refined against the neutron data and laboratory X-ray data; fits are

DOI: 10.1021/acs.inorgchem.6b01826
Inorg. Chem. 2016, 55, 12686−12695

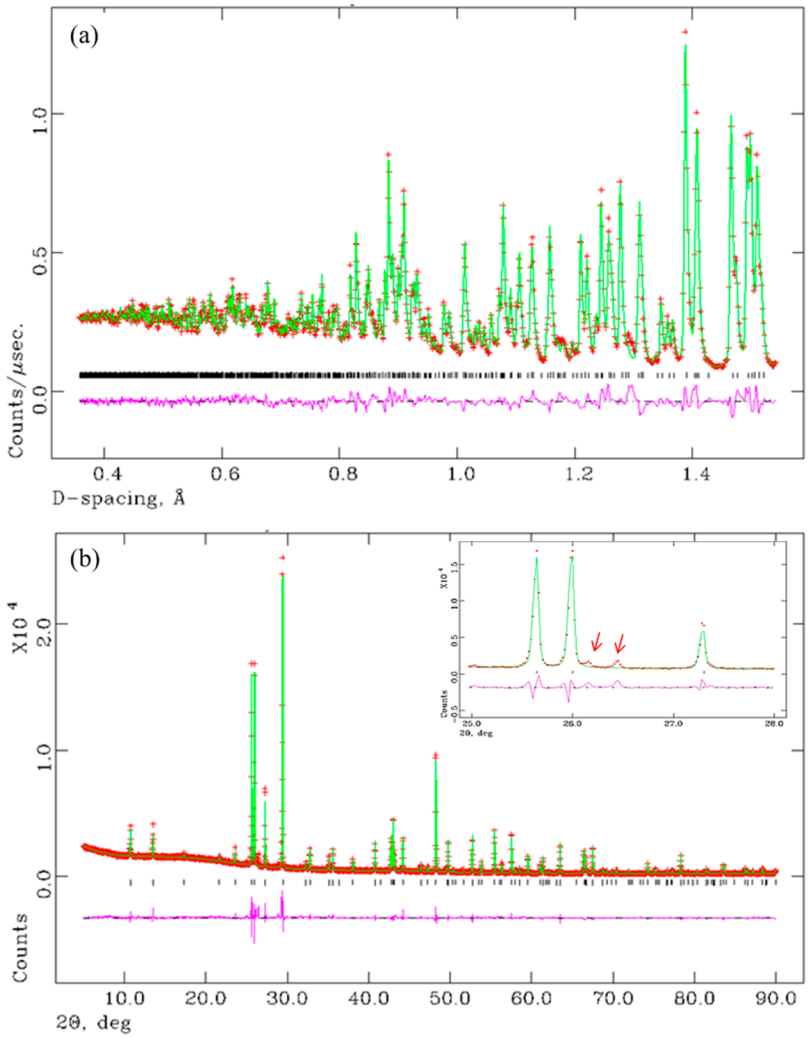

Figure 5. Simulated (green line) and experimental diffraction patterns (red dots) as well as difference pattern (purple) for $Cs_2TiNb_6O_{18}$ (solid-state reaction) using neutron diffraction data: (a) bank 6, 2θ = 154.40°; (b) laboratory XRD data. An unidentified trace impurity is indicated by the red arrows in the inset.

shown in Figure 5 and the Supporting Information, and refined parameters are given in Tables 4 and 5. The small amount of impurity is more noticeable in the neutron data but is not at a high enough level to significantly affect the refinement. All refined and derived parameters are essentially the same as those obtained from the analysis of the synchrotron X-ray diffraction data of the sample made via the aqueous precursor route, including the Cs content and slight preference for Ti on site 1. As the site occupancy and isotropic displacement parameters should be less correlated with these data, it does appear that the Cs site is fully occupied.

As noted above, the large difference in neutron scattering factors allows an accurate determination of the occupancies over the two octahedral metal sites. One might expect the Ti to fully reside in site 1 and the Nb in site 2, as they occur in a 1:6 ratio in the unit cell; in actual fact although there is a small preference for Ti on site 1 a significant amount is also found on site 2. There are several other examples of Ti/Nb oxides in the literature with more than one crystallographically independent site for the metal atoms that have been studied using neutron diffraction, and in all but one case there is a similar partial, rather than full, ordering. The first such study is that of $TiNb_2O_7$ and $Ti_2Nb_{10}O_{29}$.[26] In $TiNb_2O_7$ there are five sites where one is found to be Ti rich (64.5%): one has the expected random occupancy, and the other three are Ti-poor (14.0−26.0%). In $Ti_2Nb_{10}O_{29}$ there are six sites, and again only one is Ti-rich (40.0%), one is essentially random (16.8%), and four are Ti-poor (4.5−15.5%). In $Bi_{1.8}Sr_{2.2}Ti_{0.8}Nb_{2.2}O_{12}$ there are two sites and the Ti occupancies are 36 and 22% vs a random value of 27%.[27] In the closely related $Ba_2LaTi_2Nb_3O_{15}$ and $Ba_2NdTi_3Nb_2O_{14.5}$ the Ti shows a preference for the higher symmetry crystallographic 2c site of 45% vs 40% (random) and 80% vs 60% (random).[28,29] Finally there is one case, $Ba_2La_3NbTi_3O_{15}$, where one site is a 50:50 mix of Ti and Nb and the second is fully occupied by Ti.[30] One factor to consider that could potentially control the Ti/Nb ordering would be the second order Jahn−Teller effect, as these are both d^0 ions. According to Bhunavesh and Gopalskrishnan, smaller cation size and larger cation charge should enhance this effect and lead to a site more distorted from octahedral geometry.[31] In this study of $Cs_2TiNb_6O_{18}$ and those of $Bi_{1.8}Sr_{2.2}Ti_{0.8}Nb_{2.2}O_{12}$, $Ba_2LaTi_2Nb_3O_{15}$, $Ba_2NdTi_3Nb_2O_{14.5}$, and $Ba_2La_3NbTi_3O_{15}$ the Ti atom always prefers a less distorted site. This could be interpreted as arising from a second-order Jahn−Teller effect if the larger cation charge of Nb^{5+} has a more significant role to play in comparison to the smaller size (0.605 vs 0.64 Å) of Ti^{4+}.

DOI: 10.1021/acs.inorgchem.6b01826
Inorg. Chem. 2016, 55, 12686−12695

Table 4. Refinement Parameters, Unit Cell Parameters, Refined Atom Positions, Multiplicities, Occupancies, and Isotropic Displacement Parameters from the Refinement of Joint Neutron Diffraction and Laboratory XRD for $Cs_2TiNb_6O_{18}$ Synthesized via a Solid-State Reaction

Refinement Parameters				
	diffraction data			
			R_{wp}/%	R_p/%
Hstgm 3	neutron	bank 3	4.82	4.04
Hstgm 4	neutron	bank 4	4.73	4.04
Hstgm 5	neutron	bank 5	5.58	4.64
Hstgm 6	neutron	bank 6	4.73	3.87
Hstgm 7	laboratory	X-ray	8.83	5.92
		χ^2 = 9.193		
Lattice Parameters				
		a/Å	7.53 589(8)	
		c/Å	8.19086(10)	
		V/Å^3	402.836(11)	

Refined Atom Positions, Multiplicities, Occupancies, and Isotropic Displacement Parameters						
	x	y	z	mult	occ[a]	U_{iso}/Å^2
Cs1	0.3333	0.6667	0.63336(30)	2	0.999(4)	0.0286(7)
Nb1	0	0	0.5	1	0.728(4)	0.0045(8)
Ti1	0	0	0.5	1	0.272(4)	0.0045(8)
Nb2	0.16872(6)	−0.16872(6)	0.14496(13)	6	0.879(1)	0.0044(2)
Ti2	0.16872(6)	−0.16872(6)	0.14496(13)	6	0.121(1)	0.0044(2)
O1	0.44965(6)	−0.44965(6)	0.15967(13)	6	1	0.0074(1)
O2	0.85720(6)	−0.85720(6)	0.10177(10)	6	1	0.0074(1)
O3	0.12373(6)	−0.12373(6)	0.36269(13)	6	1	0.0074(1)

[a]Site occupancies for sites Nb1/Ti1 and Nb2/Ti2 were constrained to sum to 1.

Table 5. Interatomic Cs−O, Ti−O, and Nb−O Distances (Å) in $Cs_2TiNb_6O_{18}$ (Solid State Reaction) Calculated on the Basis of the Joint Refinement Result using Neutron Diffraction Data and Laboratory XRD Data

atoms					
		bond length/Å	mean distance/Å	valence sum (vu)	coordination
Cs1	O1	3.3015(15) (×1)	3.37 (for 9 existing Cs−O bonds)	0.84	9
Cs1	O1	3.3010(15) (×2)			
Cs1	O2	3.2999(18) (×1)			
Cs1	O2	3.3004(18) (×2)			
Cs1	O3	3.5210(18) (×1)	3.55 (for all Cs−O bonds)		
Cs1	O3	3.5215(18) (×2)			
Cs1	O3	3.80959(12) (×2)[a]			
Cs1	O3	3.80912(12) (×2)[a]			
Cs1	O3	3.80986(12) (×2)[a]			
Nb1	O3	1.9681(9) (×6)	1.97	5.14	6
Ti1	O3	1.9681(9) (×6)	1.97	3.97	6
Nb2	O1	1.9168(6) (×2)	1.99	5.00	6
Nb2	O2	2.0843(6) (×2)			
Nb2	O2	2.0491(13) (×1)			
Nb2	O3	1.8775(14) (×1)			
Ti2	O1	1.9168(6) (×2)	1.99	3.86	6
Ti2	O2	2.0843(6) (×2)			
Ti2	O2	2.0491(13) (×1)			
Ti2	O3	1.8775(14) (×1)			
				av bond valence sum (vu)	
	Nb			5.07	
	Ti			3.92	

[a]Distances considered too long for bonds.

DOI: 10.1021/acs.inorgchem.6b01826
Inorg. Chem. 2016, 55, 12686−12695

The Ti and Nb atoms adopt regular octahedral coordination. The mean Ti/Nb−O bond distances in $Cs_2TiNb_6O_{18}$ are close to the sum of ionic radii of Ti^{4+} (0.605 Å) and O^{2-} (1.40 Å) and of Nb^{5+} (0.64 Å) and O^{2-}, respectively.[32] The calculated bond valence sums (BVSs)[33] for each of the cations are given in Tables 3 and 5. For both refinements the Nb and Ti values are close to those expected, i.e. Ti^{4+} and Nb^{5+}, with those from the neutron diffraction data more precise, as expected, with the oxygen atom positions being better defined. The crystal structure of $Cs_2TiNb_6O_{18}$ consists of layers of $(M_6O_{15})_n$ sheets linked by the $(MO_3)_n$ octahedra parallel to the *c* axis by sharing corners (shown in Figure 4a); thus, cavities bounded by 21 oxygen atoms are formed. Cs cations are located between two $(M_6O_{15})_n$ layers and almost occupy the entire volume of the "O_{21}" cages, as shown in Figure 4b. The structure of $Cs_2TiNb_6O_{18}$ is rigid with no microporosity; thus, the mobility of the Cs cation is limited.[15,34] The Cs site exhibits a coordination number of 9, determined by excluding any oxygen atoms at distances that contribute less than 4% to the cation bond valence sum.[35] Although $Cs_2TiNb_6O_{18}$ does appear to be slightly underbonded with a BVS of 0.84, the high coordinate number suggests it is tightly bound in the structure. We have calculated the Cs^+ BVS values for other potential wasteforms such as the pollucites $Cs(AlSi_2O_6)$ and $Cs(FeSi_2O_6)$ and pyrochlores $CsZr_{0.5}W_{1.5}O_6$ and $CsTi_{0.25}Zr_{0.25}W_{1.5}O_6$ from published crystal structures, and these are all similarly less than 1.0 with sums of 0.70,[36] 0.67,[37] 0.92,[38] and 0.95,[38] respectively. We attempted to calculate a Cs^+ BVS for hollandite, but the complicated disorder of the Cs/Ba in the tunnels and partial occupancy of oxygen sites[7] led to unrealistically high values more suitable for Ba than for Cs, not surprisingly, as in these systems the mixed cation site is predominantly occupied by Ba.

Aqueous Durability. The normalized elemental leach rates of HIPed $Cs_2TiNb_6O_{18}$ in DI water following the MCC-1 test carried out at 90 °C are shown in Figure 6 and Table 6, and the rates from the PCT-B test are given in Table 7. It was observed that Cs leaches out at a low level but decreases with time. Low leach rates that further decrease with time were also observed in other titanate wasteforms: for example, Cs released from hollandite[39] and actinides released from pyrochlore[18,40] and zirconolite.[41] The low rate in hollandite was attributed to the presence of a passivating TiO_2 layer as a diffusion barrier formed on the particle surface.[42,43] It is expected that the same mechanism will operate here, although there was no clear evidence of this from SEM/BSE images of the monoliths before and after leaching (see the Supporting Information); this could be due to a very small amount of surface oxide after such a short period.

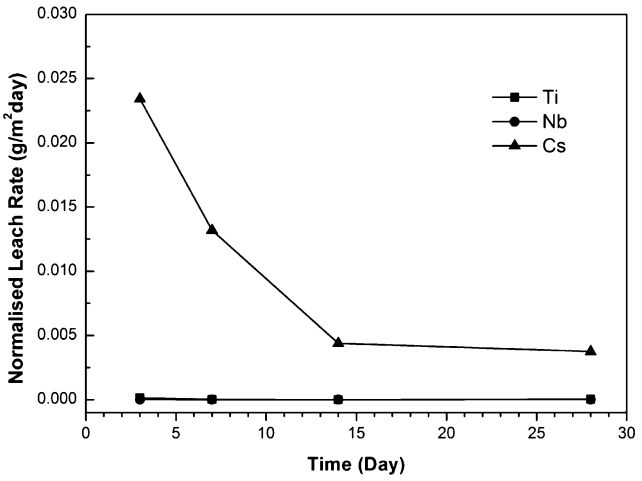

Figure 6. Normalized leach rates of Cs, Ti, and Nb as a function of time using the MCC-1 test on HIPed $Cs_2TiNb_6O_{18}$ monoliths.

Table 6. Normalized Leach Rates (g m^{-2} day^{-1}) from MCC-1 Results of HIPed $Cs_2TiNb_6O_{18}$

day	Ti	Nb	Cs
3	1.42×10^{-4}	8.55×10^{-6}	2.34×10^{-2}
7	6.14×10^{-6}	7.97×10^{-7}	1.32×10^{-2}
14	0.00×10^{a}	2.42×10^{-7}	4.38×10^{-3}
28	2.26×10^{-5}	1.09×10^{-5}	3.75×10^{-3}

[a]Concentration below the detection limit.

Table 7. Normalized Leach Rates (g m^{-2} day^{-1}) from PCT Results of HIPed $Cs_2TiNb_6O_{18}$ (7 Days Duration)

	av	esd
Ti	1.41×10^{-4}	1.083×10^{-4}
Nb	6.66×10^{-5}	4.405×10^{-5}
Cs	2.03×10^{-3}	3.589×10^{-5}

Generally, Nb and Ti are much less water soluble elements; therefore Ti and Nb showed extremely low concentrations or values below the detection limits in the leachant. The 7 day PCT-B results agree well with the MCC-1 results, even though the SA/V ratios in the two forms of leach tests differ by a factor of ∼100−250. The normalized Cs leach rates in the PCT-B tests were roughly the same order of magnitude as those in MCC-1 tests for the same duration performed. The leach rates of the most soluble alkali and alkaline-earth elements in Synroc-C at 90 °C in water are typically below 0.1 g m^{-2} day^{-1} for the first few days. In this work, we have shown that HIPed $Cs_2TiNb_6O_{18}$ has excellent chemical durability, even better than that reported in Al-rich hollandites (0.02−0.36 g m^{-2} day^{-1})[39] and Synroc-C (0.028 g m^{-2} day^{-1}).[44]

CONCLUSIONS

$Cs_2TiNb_6O_{18}$ displays excellent Cs retention due to its condensed structure leading to no diffusion pathways where Cs can migrate and a chemical composition that is highly insoluble. In comparison with the MCC-1 and PCT-B results of hollandite,[39] the material targeted for Cs sequestration in Synroc, HIPed $Cs_2TiNb_6O_{18}$ shows 1−3 orders of magnitude better Cs retention from the MCC-1 results and 3−4 orders of magnitude better from the PCT-B results. In practice, $Cs_2TiNb_6O_{18}$ is very comparable with hollandite or is even more leach resistant. For long-term considerations, $Cs_2TiNb_6O_{18}$ is a promising candidate for Cs immobilization not only due to the low leach rate but also because it should retain Ba^{2+} produced by transmutation of Cs^+, as charge compensation to trap the electron emitted during the β decay could occur via reduction of Ti^{4+} to Ti^{3+} or of Nb^{5+} to Nb^{4+}. $Cs_2TiNb_6O_{18}$ was obtained via both ceramic and aqueous precursor methods. The aqueous precursor method provides an easier and more efficient approach to produce a highly crystalline and pure material. The structural studies based on Rietveld refinements using synchrotron X-ray and neutron diffraction data support a structure with high-coordination-number Cs atoms located in the cavities, indicating that Cs atoms are tightly bonded in the structure. Both MCC-1 and PCT-B test results indicate the potential of

DOI: 10.1021/acs.inorgchem.6b01826
Inorg. Chem. 2016, 55, 12686−12695

$Cs_2TiNb_6O_{18}$ as a highly chemically durable wasteform for Cs immobilization.

■ ASSOCIATED CONTENT

Supporting Information

The Supporting Information is available free of charge on the ACS Publications website at DOI: 10.1021/acs.inorgchem.6b01826.

SEM/BSE images of $Cs_2TiNb_6O_{18}$ powder, powder X-ray diffraction patterns of the monoliths before and after leach testing, SEM/BSE images of the monoliths before and after leach testing, and observed, calculated, and difference profiles from the Rietveld refinement of the neutron diffraction data from three detector banks (PDF)

Crystallographic data for $Cs_2TiNb_6O_{18}$ (CIF)

■ AUTHOR INFORMATION

Corresponding Authors

*E-mail for T.-Y.C.: t.chen.3@bham.ac.uk.

*E-mail for J.A.H.: j.a.hriljac@bham.ac.uk.

ORCID

Joseph A. Hriljac: 0000-0001-9978-6530

Notes

The authors declare no competing financial interest.

■ ACKNOWLEDGMENTS

We gratefully acknowledge Dr. Jackie Deans for technical assistance. This research was partially funded by the Nuclear Decommissioning Authority through a studentship bursary to T.-Y.C. and research sponsorship to N.C.H. We gratefully acknowledge the National Nuclear Laboratory (NNL), the EPSRC (EP/L014041/1, DISTINCTIVE), and NCH the Royal Academy of Engineering for additional research sponsorship. We thank Diamond Light Source for access to beamline I11 (EE12092) and the ISIS Pulsed Neutron and Muon Source supported by the Science and Technology Facilities Council for access to GEM that contributed to the results presented here. The Bruker D8, Bruker S8, and Netzsch STA 449FA instruments used in this research were obtained through Birmingham Science City: Creating and Characterizing Next Generation Advanced Materials (West Midlands Centre for Advanced Materials Project 1), with support from Advantage West Midlands (AWM) and partially funded by the European Regional Development Fund (EDRF). The Advanced Materials Facility is part of the Centre for Chemical and Materials Analysis in the School of Chemistry at the University of Birmingham. Data associated with the results shown in this paper are accessible from the University of Birmingham Archive: http://epapers.bham.ac.uk/2217/.

■ REFERENCES

(1) Kobayashi, T.; Nagai, H.; Chino, M.; Kawamura, H. Source Term Estimation of Atmospheric Release due to the Fukushima Dai-ichi Nuclear Power Plant Accident by Atmospheric and Oceanic Dispersion Simulations. *J. Nucl. Sci. Technol.* **2013**, *50*, 255−264.

(2) Chino, M.; Nakayama, H.; Nagai, H.; Terada, H.; Katata, G.; Yamazawa, H. Preliminary Estimation of Release Amounts of ^{131}I and ^{137}Cs Accidentally Discharged from the Fukushima Daiichi Nuclear Power Plant into the Atmosphere. *J. Nucl. Sci. Technol.* **2011**, *48*, 1129−1134.

(3) Saito, K.; Tanihata, I.; Fujiwara, M.; Saito, T.; Shimoura, S.; Otsuka, T.; Onda, Y.; Hoshi, M.; Ikeuchi, Y.; Takahashi, F.; Kinouchi, N.; Saegusa, J.; Seki, A.; Takemiya, H.; Shibata, T. Detailed Deposition Density Maps Constructed by Large-scale Soil Sampling for Gamma-ray Emitting Radioactive Nuclides from the Fukushima Dai-ichi Nuclear Power Plant Accident. *J. Environ. Radioact.* **2015**, *139*, 308−319.

(4) Xu, Y.; Wen, Y.; Grote, R.; Amoroso, J.; Nickles, L. S.; Brinkman, K. S. A-site Compositional Effects in Ga-doped Hollandite Materials of the Form $Ba_xCs_yGa_{2x+y}Ti_{8-2x-y}O_{16}$: Implications for Cs Immobilization in Crystalline Ceramic Waste Forms. *Sci. Rep.* **2016**, *6*, 27412.

(5) Watanabe, M.; Fujiki, Y.; Kanazawa, Y.; Tsukimura, K. The Effects of Cation Substitution on the Hollandite-type Structure. *J. Solid State Chem.* **1987**, *66*, 56−63.

(6) Abe, H.; Satoh, A.; Nishida, K.; Abe, E.; Naka, T.; Imai, M.; Kitazawa, H. Electrochemical Immobilization of Cs in Single-crystalline SYNROC. *J. Solid State Chem.* **2006**, *179*, 1521−1524.

(7) Leinekugel-Le-Cocq, A. Y.; Deniard, P.; Jobic, S.; Cerny, R.; Bart, F.; Emerich, H. Synthesis and Characterization of Hollandite-type Material Intended for the Specific Containment of Radioactive Cesium. *J. Solid State Chem.* **2006**, *179*, 3196−3208.

(8) Bursill, L. A.; Smith, D. J. Electron Irradiation Effects in (Cs,Ba)-hollandites. *J. Solid State Chem.* **1987**, *69*, 343−354.

(9) Tang, M.; Tumurugoti, P.; Clark, B.; Sundaram, S. K.; Amoroso, J.; Marra, J.; Sun, C.; Lu, P.; Wang, Y. Q.; Jiang, Y. B. Heavy Ion Irradiations on Synthetic Hollandite-type Materials: $Ba_{1.0}Cs_{0.3}A_{2.3}Ti_{5.7}O_{16}$ (A = Cr, Fe, Al). *J. Solid State Chem.* **2016**, *239*, 58−63.

(10) Ewing, R. C.; Weber, W. J.; Clinard, F. W. Radiation Effects in Nuclear Waste Forms for High-level Radioactive Waste. *Prog. Nucl. Energy* **1995**, *29*, 63−127.

(11) Smith, F. G.; Lee, S. Y.; King, W. D.; McCabe, D. J. Comparisons of Crystalline Silicotitanate and Resorcinol Formaldehyde Media for Cesium Removal by In-tank Column Processing. *Sep. Sci. Technol.* **2008**, *43*, 2929−2942.

(12) Walker, J. F.; Taylor, P. A.; Lee, D. D. Cesium Removal from High-pH, High-salt Wastewater using Crystalline Silicotitanate Sorbent. *Sep. Sci. Technol.* **1999**, *34*, 1167−1181.

(13) Chen, T.-Y.; Hriljac, J. A.; Gandy, A. S.; Stennett, M. C.; Hyatt, N. C.; Maddrell, E. R. Thermal Conversion of Cs-exchanged IONSIV IE-911 into a Novel Caesium Ceramic Wasteform by Hot Isostatic Pressing. *MRS Online Proc. Libr.* **2013**, *1518*, 67−72.

(14) Desgardin, G.; Robert, C.; Groult, D.; Raveau, B. New Structural Family - Titanoniobates and Titanotantalates $A_2Nb_6TIO_{18}$ and $A_2Ta_6TlO_{18}$. *J. Solid State Chem.* **1977**, *22*, 101−111.

(15) Desgardin, G.; Robert, C.; Raveau, B. Etude du Comportement du Thallium dans de Nouvelles Structures a Tunnels Entrecroises: Les Oxydes $Tl_2Nb_6TiO_{18}$ et $Tl_2Ta_6TiO_{18}$. *Mater. Res. Bull.* **1978**, *13*, 621−626.

(16) Boccaccini, A. R.; Atiq, S.; Grimes, R. W. Hot-pressed Glass Matrix Composites Containing Pyrochlore Phase Particles for Nuclear Waste Encapsulation. *Adv. Eng. Mater.* **2003**, *5*, 501−508.

(17) Ewing, R. C.; Weber, W. J.; Lian, J. Nuclear Waste Disposal-pyrochlore $A_2B_2O_7$: Nuclear Waste Form for the Immobilization of Plutonium and "minor" Actinides. *J. Appl. Phys.* **2004**, *95*, 5949−5971.

(18) Zhang, Y.; Li, H.; Moricca, S. Pyrochlore-structured Titanate Ceramics for Immobilisation of Actinides: Hot Isostatic Pressing (HIPing) and Stainless Steel/Waste Form Interactions. *J. Nucl. Mater.* **2008**, *377*, 470−475.

(19) Lumpkin, G. R. Ceramic waste forms for actinides. *Elements* **2006**, *2*, 365−372.

(20) Balmer, M. L.; Su, Y. L.; Xu, H. W.; Bitten, E.; McCready, D.; Navrotsky, A. Synthesis, Structure Determination, and Aqueous Durability of $Cs_2ZrSi_3O_9$. *J. Am. Ceram. Soc.* **2001**, *84*, 153−160.

(21) Larson, A. C.; von Dreele, R. B. *GSAS program*, 1994

(22) Brown, I. D.; Altermatt, D. Bond-valence Parameters Obtained from a Systematic Analysis of the Inorganic Crystal Structure Database. *Acta Crystallogr., Sect. B: Struct. Sci.* **1985**, *41*, 244−247.

(23) Standard Test Method for Static Leaching of Monolithic Waste Forms for Disposal of Radioactive Waste. In ASTM International,

DOI: 10.1021/acs.inorgchem.6b01826
Inorg. Chem. 2016, 55, 12686−12695

Standard Test Method for Static Leaching of Monolithic Waste Forms for Disposal of Radioactive Waste, 1998.
(24) Standard Test Methods for Determining Chemical Durability of Nuclear, Hazardous, and Mixed Waste Glasses and Multiphase Glass Ceramics: The Product Consistency Test (PCT). In ASTM International, Standard Test Methods for Determining Chemical Durability of Nuclear, Hazardous, and Mixed Waste Glasses and Multiphase Glass Ceramics: The Product Consistency Test (PCT), 2002; Vol. C, 1285-02.
(25) NIST Center for Neutron Research, Neutron scattering Lengths and Cross Sections; http://www.ncnr.nist.gov/resources/n-lengths/.
(26) Von Dreele, R. B. V.; Cheetham, A. K. The Structures of Some Titanium-Niobium Oxides by Powder Neutron Diffraction. *Proc. R. Soc. London, Ser. A* **1974**, *338*, 311−326.
(27) Hervoches, C. H.; Lightfoot, P. Cation Disorder in Three-Layer Aurivillius Phases: Structural Studies of $Bi_{2-x}Sr_{2+x}Ti_{1-x}Nb_{2+x}O_{12}$ ($0 < x < 0.8$) and $Bi_{4-x}La_xTi_3O_{12}$ ($x = 1$ and 2). *J. Solid State Chem.* **2000**, *153*, 66−73.
(28) Miles, G. C.; Stennett, M. C.; Reaney, I. M.; West, A. R. Temperature-dependent Crystal Structure of Ferroelectric $Ba_2LaTi_2Nb_3O_{15}$. *J. Mater. Chem.* **2005**, *15*, 798−802.
(29) Prades, M.; Masó, N.; Beltrán, H.; Cordoncillo, E.; West, A. R. Synthesis, Structural Characterization, and Electrical Properties of New Oxygen-Deficient Tetragonal Tungsten Bronzes $Ba_2NdTi_{2+x}Nb_{3-x}O_{15-x/2}$. *Inorg. Chem.* **2013**, *52*, 1729−1736.
(30) De Paoli, J. M.; Alonso, J. A.; Carbonio, R. E. Synthesis and Structure Refinement of Layered Perovskites $Ba_{5-x}La_xNb_{4-x}Ti_xO_{15}$ ($x = 0$, 1, 2, 3 and 4) Solid Solutions. *J. Phys. Chem. Solids* **2006**, *67*, 1558−1566.
(31) Bhuvanesh, N. S. P.; Gopalakrishnan, J. Solid-state Chemistry of Early Transition-metal Oxides Containing d^0 and d^1 cations. *J. Mater. Chem.* **1997**, *7*, 2297−2306.
(32) Shannon, R. D. Revised Effective Ionic-radii and Systematic Studies of Interatomic Distances in Halides and Chalcogenides. *Acta Crystallogr., Sect. A: Cryst. Phys., Diffr., Theor. Gen. Crystallogr.* **1976**, *32*, 751−767.
(33) Altermatt, D.; Brown, I. D. The Automatic Searching for Chemical-bonds in Inorganic Crystal-structures. *Acta Crystallogr., Sect. B: Struct. Sci.* **1985**, *41*, 240−244.
(34) Robert, C.; Desgardin, G.; Raveau, B. Ion Exchange Properties of the Cxides $Tl_2M_7O_{18}$: the Oxides $(H_3O)_2M_7O_{18}$ and $A_2M_7O_{18}\cdot 2H_2O$ (A = K, Ag). *J. Inorg. Nucl. Chem.* **1979**, *41*, 893−894.
(35) Brown, I. D. *The Chemical Bond in Inorganic Chemistry: The Bond Valence Model*; Oxford University Press: Oxford, U.K., 2006.
(36) Yanase, I.; Kobayashi, H.; Shibasaki, Y.; Mitamura, T. Tetragonal-to-cubic Structural Phase Transition in Pollucite by Low-temperature X-ray Powder Diffraction. *J. Am. Ceram. Soc.* **1997**, *80*, 2693−2695.
(37) Bell, A. M. T.; Henderson, C. M. B. Rietveld Refinement of the Structures of Dry-synthesized $MFe^{III}Si_2O_6$ leucites (M = K, Rb, Cs) by Synchrotron X-ray Powder Diffraction. *Acta Crystallogr., Sect. C: Cryst. Struct. Commun.* **1994**, *50*, 1531−1536.
(38) Whittle, K. R.; Lumpkin, G. R.; Ashbrook, S. E. Neutron Diffraction and MAS NMR of Cesium Tungstate Defect Pyrochlores. *J. Solid State Chem.* **2006**, *179*, 512−521.
(39) Carter, M. L.; Gillen, A. L.; Olufson, K.; Vance, E. R. HIPed Tailored Hollandite Waste Forms for the Immobilization of Radioactive Cs and Sr. *J. Am. Ceram. Soc.* **2009**, *92*, 1112−1117.
(40) Finkeldei, S.; Brandt, F.; Rozov, K.; Bukaemskiy, A. A.; Neumeier, S.; Bosbach, D. Dissolution of ZrO_2 Based Pyrochlores in the Acid pH Range: A Macroscopic and Electron Microscopy Study. *Appl. Geochem.* **2014**, *49*, 31−41.
(41) Zhang, K. B.; Wen, G. J.; Zhang, H. B.; Teng, Y. C. Self-propagating High-temperature Synthesis of CeO_2 Incorporated Zirconolite-rich Waste Forms and the Aqueous Durability. *J. Eur. Ceram. Soc.* **2015**, *35*, 3085−3093.
(42) Carter, M. L.; Vance, E. R.; Mitchell, D. R. G.; Hanna, J. V.; Zhang, Z.; Loi, E. Fabrication, Characterization, and Leach Testing of Hollandite, (Ba,Cs) $(Al,Ti)_2Ti_6O_{16}$. *J. Mater. Res.* **2002**, *17*, 2578−2589.
(43) Pham, D. K.; Myhra, S.; Turner, P. S. The Surface Reactivity of Hollandite in Aqueous Solution. *J. Mater. Res.* **1994**, *9*, 3174−3182.
(44) Smith, K. L.; Lumpkin, G. R.; Blackford, M. G.; Day, R. A.; Hart, K. P. Durability of Synroc. *J. Nucl. Mater.* **1992**, *190*, 287−294.

DOI: 10.1021/acs.inorgchem.6b01826
Inorg. Chem. 2016, 55, 12686−12695